Journal of the Brazilian Society of Mechanical Sciences and Engineering (2018) 40:382
https://doi.org/10.1007/s40430-018-1303-5

TECHNICAL PAPER

Experimental and numerical investigation of the fracture behavior of adhesive shear tests single lap joints

M. C. Ezzine[1] · A. Amiri[1] · M. Tarfaoui[2]

Received: 1 November 2017 / Accepted: 10 July 2018 / Published online: 17 July 2018

Abstract

This work aims to establish a finite element model to simulate the behavior in cracking failure of a shear test of a single lap joint. The interest of having a satisfactory finite element model is to be able to use it to simulate the cases that have not been the subject of experimental tests. A cohesive zone model (CZM) was used to model the propagation of cracks in bonded joints, using a bilinear traction–separation law implemented in the finite element code Abaqus. The cohesive zone is represented by a row of cohesive elements where the progression of the crack will take place. The parameters of the cohesive law of an adhesive "Adekit A140" were determined by fracture tests, performed on DCB and ENF tests. A damage initiation criterion and a mixed-mode failure criterion are used, respectively, to initiate and perform damage to the interfaces. Two numerical models of single lap joint were tested. In the first model (CZMi), the cohesive zone is represented by a row of cohesive elements placed along a single interface (adhesive–substrate) and the second interface of the model being left intact. In the second model (CZMii), the cohesive elements are placed along the two interfaces of between adhesive and substrate. In this case, the cohesive zone comprises two rows of cohesive elements. Experimental shear tests were performed on single lap joints bonded with Adekit A140 adhesive to determine the force–displacement curve. The numerical model using a single row of cohesive elements has a force–displacement curve shifted backward of the experimental force–displacement curve. It shows a greater initial rigidity and less resistance to crack propagation in the joints. The force–displacement curve of the numerical model using two rows of cohesive elements coincides with the experimental force–displacement curve. The numerical force–displacement curve shows good initial stiffness and good resistance to crack propagation in joints. These latest numerical results (two rows of cohesive elements) are in good agreement with the experimental results and allow us to validate the numerical model applied to shear tests of bonded joints.

Keywords Single lap joint · Failure · Cohesive zone model · DCB and ENF tests · Validation

1 Introduction

Nowadays, bonding is an assembly technique with high mechanical performance, widely used in several industrial sectors, especially for the automotive and aeronautics. Adhesives are effective when they work in shear. The single overlap joint is the most studied type of bonded joint in order to test its mechanical properties and therefore the strength of the adhesives under shear conditions. This choice is dictated by its simple geometry and ease of implementation. The finite element method has been widely used to predict the behavior of bonded joints [1–4]. Its biggest advantage is that it is very easy to modify the boundary conditions and geometries, to introduce nonlinear behavior, analyze structures made of different materials [5, 6] and to create complex parametric studies with a three-dimensional modeling [7–9]. These models are widely used to predict the distribution of stresses in the assemblies, and associated with a failure criterion of the adhesive, of predicting failure thereof. Indeed, for metallic materials, attention is focused exclusively on the adhesive

Technical Editor: Paulo de Tarso Rocha de Mendonça.

✉ M. C. Ezzine
ezzine_chamseddine@yahoo.fr

[1] Laboratoire de mécanique et Physique des Matériaux, Université de Sidi Bel-Abbès, Sidi Bel-Abbès, Algeria

[2] IRDL (CNRS-FRE-3744), Institut de recherché Dupuy de Lôme, ENSTA Bretagne, 29200 Brest, France

which by its mechanical properties remains the weak link in the assembly. Cohesive zone models (CZM) were used for predicting the strength of adhesive joints, as an addition to the finite element analysis that allows simulation of the initiation and propagation of damage in a raw material or interfaces between different materials [10–12]. This method is widely used to model delamination at the substrate/adhesive interface in the bonded joints [13]. Borg [14] developed a model using cohesive elements, and the model was validated by conventional tests of fracture mechanics (DCB, ENF) and applied to a single lap joint. The traction–separation law with a triangular shape (bilinear law) was established in this work. The adhesive bonds are particularly suited to cracking tests where the analysis is based on an energy balance. The values of the strain energy release rate in tension and shear (G_{nc}, G_{sc}, respectively) are needed. The cohesive stresses in tension and shear (t_{no} and t_{so}, respectively) are also required, relating to the initiation of damage, which means the end of the elastic behavior and the beginning of the damage. To define cohesive parameters (G_{nc}, G_{sc}, t_{no} and t_{so}), the DCB and ENF tests were performed, which provided conclusive results [15, 16]. An analytical analysis is necessary, using analytic relations to operate in a simple way the results of the tests. The proposed methods of analysis are based on linear elastic fracture mechanics (LEFM). These methods consist of an approach with beam theory [17, 18] or an experimental method of compliance calibration [19]. These techniques are used to determine fracture energies G_c and draw resistance curves (R curves).

In this article, we studied experimentally the behavior of a single lap joint using adhesive ADEKIT A140. The experimental work was completed by numerical modeling using cohesive zone models. DCB and ENF tests were conducted to characterize the interface between the adhesive and the substrates. The tensile testing machine type "Zwick" was performed and equipped with a camera by high performance (Retiga). The complacency of the system was estimated by means of analytical relations from which are deduced the fracture energies of the interfaces (steel-adhesive) in mode I and II (G_{Ic}, G_{IIc}, respectively) and the traction forces in tension and shear (t_n, t_s, respectively).

To correctly simulate the cracking failure behavior of a shear test of a bonded joint with an adhesive "ADEKIT A140" under a bilinear traction–separation law, two models of cohesive zones (CZMi and CZMii) were used, using one or two rows of cohesive elements. The model using two rows of cohesive elements presents results consistent with the experimental results.

2 Experimental study

2.1 Materials

2.1.1 Adhesive properties "ADEKIT A140"

The adhesive used is a two-component epoxy ADEKIT A140. To determine the adhesive's behavior law, tensile tests were carried out on dumbbell specimens manufactured according to ISO527-2, Fig. 1, on a Zwick machine with a traveling speed of the cross of 0.1 mm/min at room temperature. Four tests were performed. The results obtained on the different samples tested show a similar behavior.

A typical traction curve "axial stress-axial strain" is shown in Fig. 2. The mechanical properties of ADEKIT A140 are shown in Table 1.

2.1.2 Substrate properties

Steel plates with a thickness of 2 mm were cut to form the substrates. The adhesive joints are made between two metal substrates steel E24 provided by the company FAMAG industry. Steel has a large enough strength to avoid exceeding its elastic limit during mechanical testing. The mechanical properties of the steel E24 are shown in Table 2.

2.2 Geometry of specimens

2.2.1 Specimen for lap shear testing

The specimens are single-lap bonded joints for use on a pulling machine. Figure 3 shows the geometry of the joint. The test specimens consist of two metal substrates assembled with an adhesive. The ends are reinforced by beads which are positioned so that the tensile force is applied in the plane of the adhesive joint during assembly in the jaw.

The surfaces to be bonded were initially degreased, then treated by sandblasting and finally cleaned with acetone. Teflon strips have been put in place to define the bonding surface and shims to adjust the thickness of the adhesive joint. The assemblies are then placed in a holding mold to be cross-linked with the ambient air.

2.2.2 Specimen for mode I (DCB)

The test most used and most simple to perform for the characterization of resistance to delamination in mode I is the test specimen DCB. The DCB test pieces were fabricated from steel E24 substrates. The substrates are

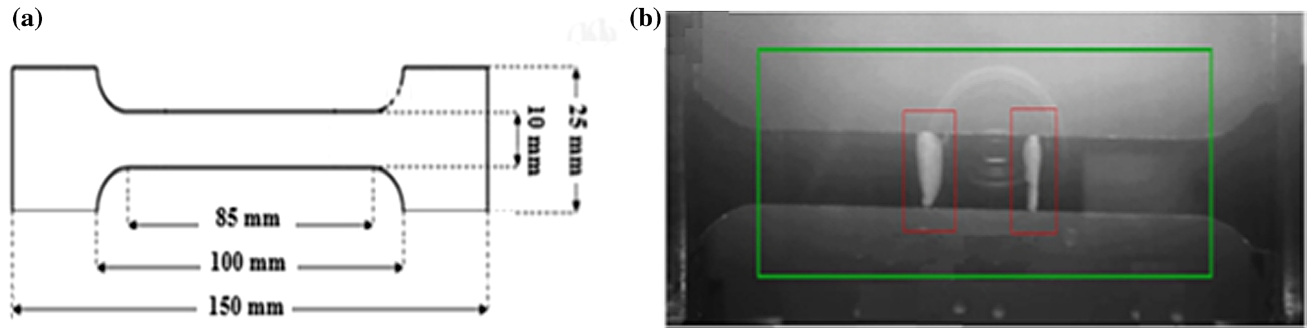

Fig. 1 Geometry of dumbbell specimens. **a** Geometry of dumbbell and **b** specimen in tested

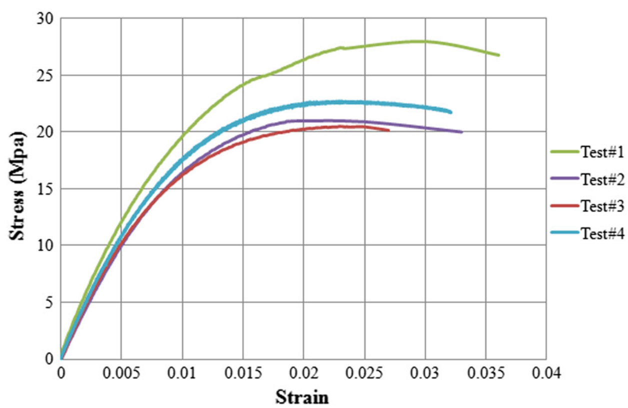

Fig. 2 Mechanical behavior of adhesive "ADEKIT A140"

connected by a layer of adhesive "Adekit A140" of thickness 0.2 mm, Fig. 4. A pre-crack (a_0) is performed by positioning a release film at the edge of substrate. This length is calculated between the tip of the crack and the point of application of the load. The surfaces to be bonded were treated with fine sanding and polishing to the past for a brazing. The last step involves cleaning with acetone to remove the oxide layer. The upper end of the DCB specimen is subjected to a quasi-static loading. The dimensions of the DCB test specimen are shown in Table 3, or "b" is the width of the specimen [20].

Table 2 Mechanical characteristics of the steel E 24

Properties	Values
Young's modulus (GPa)	210
Tensile strength (MPa)	350
Yield strength (MPa)	250
Shear modulus (Gpa)	81
Poisson's ratio	0.3

2.2.3 Specimen for mode II (ENF)

The ENF specimen consists of two steel E24 plates. The plates were bonded along 160 mm using Adekit A140 adhesive 0.2 mm thick, Fig. 5. The metal plates were mechanically treated and cleaned with acetone. Pre-cracks are made at the adherent/adhesive interface, and steel calls were inserted to ensure the thickness of the adhesive. The curing was carried out for 3 days at room temperature under pressure. Table 4 shows the dimensions of the ENF test piece. "b" is the width of the specimen.

Table 1 Mechanical properties of ADEKIT A140

	Young's modulus E (MPa)	Poisson coefficient v	Yield stress σ_e (MPa)	Failure stress σ_r (MPa)	Deformation at failure ε_r (%)
Test 1	3177	0.35	7.05	27.3	0.0036
Test 2	2272	0.35	6.72	20.96	0.0033
Test 3	2560	0.35	7.22	20.1	0.0027
Test 4	2631	0.35	7.1	22.5	0.00325
Average	2660	0.35	7.022	22.715	0.0032
Standard deviation	378.01	0.00	0.21	2.78	0.0003

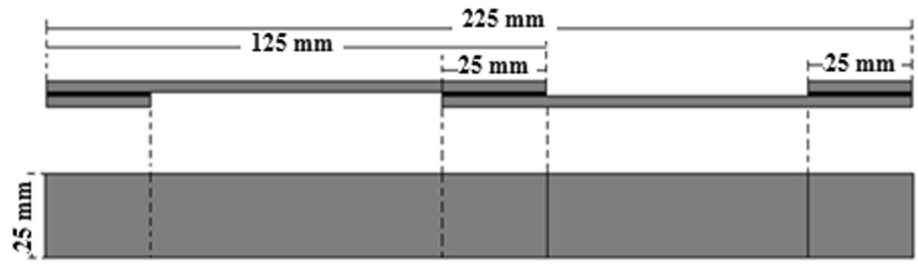

Fig. 3 Geometry of the bonded joint

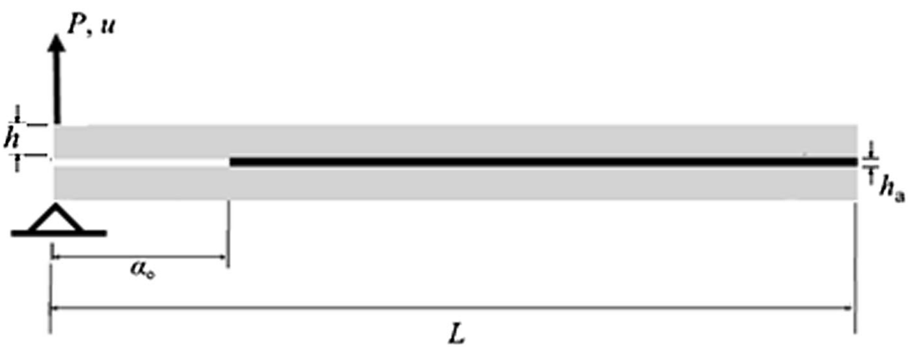

Fig. 4 Geometry of the DCB specimen

Table 3 Dimension of the DCB specimen

Dimension	L	a_0	b	h	h_a
Value (mm)	120	40	25	3	0.2

Table 4 Dimension of the specimen ENF

Dimension	L	h	a_0	b	h_a
Value (mm)	160	3	40	25	0.2

2.3 Mechanical tests

2.3.1 DCB tests

The tests were performed on an electromechanical machine ADAMEL type test of 100 kN capacity. Crack growth is recorded using a digital camera "Retiga 1300." Figure 6 shows the DCB joined at the test court. The experimental results of the DCB tests are shown in Fig. 13a. The critical energy release rate (G_{Ic}) values are calculated as a result using different methods.

Methods of analysis of a DCB test are based on the compliance method. These require that the values of the load "*P*," the relative displacement "*d*" and the crack length "*a*" to be recorded during the test. The energy release rate is calculated using the relationship of Irwin-Kies [21]:

$$G_I = \frac{1}{b}\frac{\partial U}{\partial a} = \frac{P^2}{2b}\frac{\partial C}{\partial a}, \quad (1)$$

where U is the elastic energy stored in the structure, b the width of the specimen and $C = d/P$ is the compliance.

Four methods are presented in our calculations:

2.3.1.1 MBT 1 (modified beam theory 1) The modified beam theory models the DCB specimen as a simple cantilever beam based on the Timoshenko beam theory:

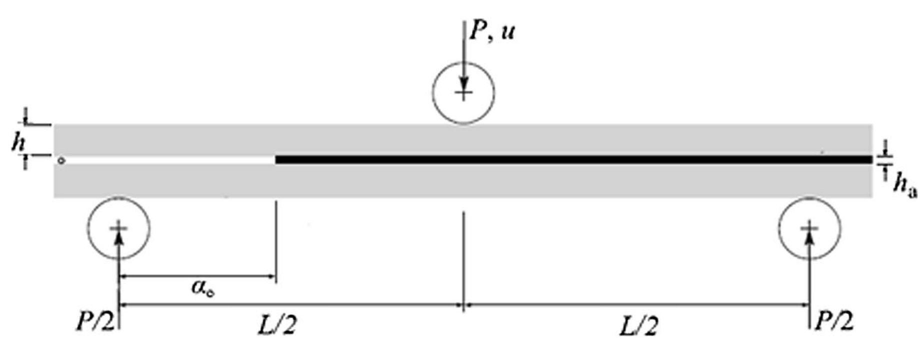

Fig. 5 Geometry of the specimen ENF

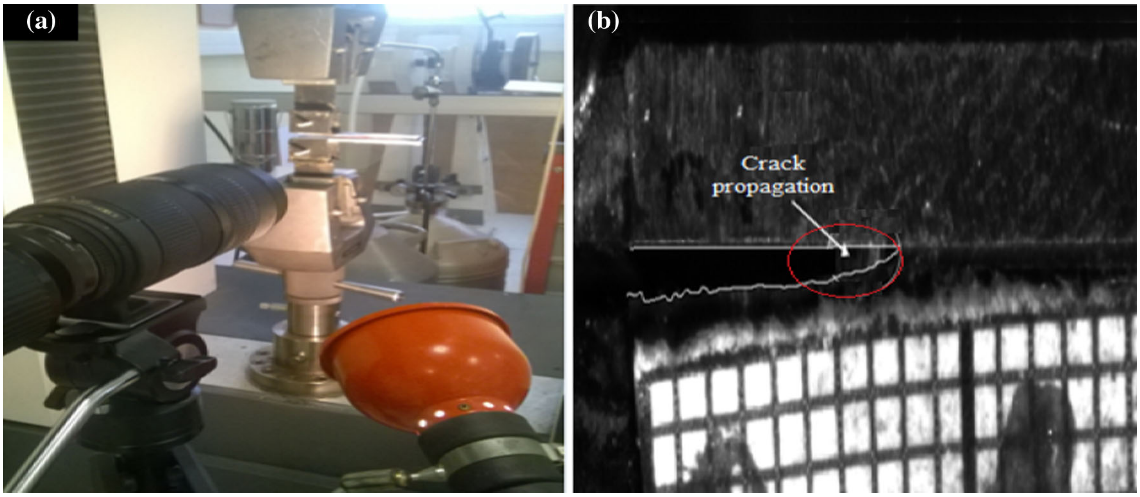

Fig. 6 DCB test apparatus. **a** DCB test and **b** test specimens during test

$$G_{\mathrm{I}} = \frac{3P\delta}{2ba}, \tag{2}$$

where "P" is the load to give a "δ" displacement, "b" is the specimen width and "a" is the crack length. This theory calculates the G_{I} considering the compliance of the cracked beam. This basic law is easy to implement but can be inaccurate.

2.3.1.2 MBT 2 (modified beam theory 2) In the modified beam theory 2, we take into account the rotation of the crack front as well as the partially cracked interface to account for the fiber bridging.

$$G_{\mathrm{I}} = \frac{3P\delta}{2b(a+|\Delta|)} \cdot \frac{F}{N} \tag{3}$$

This theory takes into account the rotation of the crack tip. Also it was seen during the experiments that the DCB specimens underwent large displacements to propagate the crack; hence, a correction factor should be included to take into account the turning effects of the U blocks.

$$N = 1 - \left(\frac{l_2}{a}\right)^3 - \frac{9}{8}\left[1 - \left(\frac{l_2}{a}\right)^2\right]\frac{l_1\delta}{a^2} - \frac{9}{35}\left(\frac{\delta}{a}\right)^2, \tag{4}$$

$$F = 1 - \frac{3}{10}\left(\frac{\delta}{a}\right)^2 - \frac{3}{2}\left(\frac{l_1\delta}{a^2}\right), \tag{5}$$

where "P" is the force applied, "δ" the displacement of the two beams, "b" the width of the specimen, "a" the length of the crack, "Δ" the crack front rotation correction factor, "l_1" the distance of the loading pin to the mid plane of the specimen and "l_2" the distance from the center of the pin to the end of the U-block.

2.3.1.3 CC (compliance calibration method) With the compliance calibration method, the compliance is considered to be a function of the crack beam. It was proposed by Berry [22]. The formulation for G_{I} is thus given by (6).

$$G_{\mathrm{I}} = \frac{nP\delta}{2ba} \cdot \frac{F}{N}, \tag{6}$$

where n determined experimentally is the slope of Log (C/N) = f (log (a)).

2.3.1.4 MCC (modified compliance calibration method) Modified compliance method (MCC) is expressed by (7):

$$G_{\mathrm{I}} = \frac{3P^2C^{2/3}}{2A_1bh}, \tag{7}$$

where A_1 is the director coefficient (a/h) = $f\,(C/N)^{1/3}$).

The study of these different methods (MBT1, MBT2, CC and MCC) aims to compare and give the best possible method to determine the critical energy release rate G_{IC}. The evolution of the energy release rate G_{I} along the length of the crack "a" was calculated (R curves) and is shown in Fig. 7. We note that the different curves of (G_{I}) converge on the interval (85, 105 mm) of the crack length "a," Fig. 7. This value represents the critical energy release rate G_{IC}. Table 5 summarizes G_{IC} for the different methods.

2.3.2 ENF tests

The ENF tests were carried out on the same traction machine as the DCB test "ADAMEL." The specimen is biased by a displacement of the jack in the middle of the joint perpendicular to the plane of the adhesive joint. The load and displacement are recorded with sensors of the machine, while crack growth is recorded using a digital

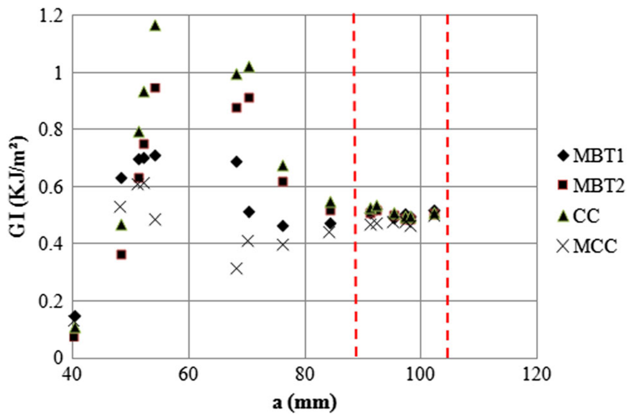

Fig. 7 Energy release rate G_I based on the crack propagation (R curves)

Table 5 Evaluation of critical strain energy release rate (G_{Ic}) for pure mode I

	MBT1	MBT2	CC	MCC
G_{Ic} (kJ/m^2)	0.50	0.50	0.51	0.48
Std (kJ/m^2)	0.01	0.01	0.02	0.02

camera. The most important parameter in an ENF test is the ratio a_0/L. It is the latter which introduces the stability condition of the test. The ratio which contributes to stable crack propagation is 0.25. The critical energy release rate (G_{IIc}) value is calculated as a result using different methods.

Based on the beam theory, there are different analytical approaches that have been formulated for the calculation of the strain energy release rate in mode II "$G_{II.}$"

2.3.2.1 Beam theory (BT) In general, the mode II SERR is given by $G = \frac{P^2}{2b}\frac{dC}{da}$, where G can be calculated from Eqs. (8).

$$G_{II} = \frac{9a^2P^2}{16E_{11}b^2h^3} \tag{8}$$

2.3.2.2 Shearing height theory (SH)

$$G_{II} = \frac{9a^2P^2}{16E_{11}b^2h^3}\left(1 + 0.2\frac{E_1}{G_{13}}\left(\frac{h}{a}\right)^2\right), \tag{9}$$

where "G_{13}" is the shearing modulus which takes into account the shearing deformation of the crack front in the calculation of the mode II SERR.

2.3.2.3 Compliance calibration (CC)

$$G_{II} = \frac{1.5ma^2P^2}{b^2}, \tag{10}$$

where "m" is a coefficient which depends on the function "$C = f(a^3)$."

For the ENF test, the results of the different methods of analysis are shown in Fig. 8, which show the evolution of G_{II} as a function of the length of the crack "a."

Figure 8 shows the different G_{II} curves, which join and stabilize along a horizontal line portion, which represents the critical energy release rate (G_{IIc}). G_{II} was calculated and is shown in Table 6 with the different methods.

2.3.3 Shear tests

The test is carried out on a traction machine type Zwick-Roll with a loading speed of 0.1 mm/min. The behavior of the test piece during the shear test is shown in Fig. 9. The curve shows an initial elastic behavior until reaching the breaking force. Then, an acceleration of the deformation of the joint is observed and a decrease in the force until the failure of the specimen.

The bonded single lap joints after rupture are shown in Fig. 10. The fracture facets for the DCB and SLJ joints show that adhesive failure of the joints has occurred.

3 Numerical study

3.1 Finite element simulation

DCB (Mode I), ENF (Mode II) and shear tests were experimentally tested. Comparison between numerical and experimental results of cracking allows us to validate a numerical model, which will be applied subsequently to cases of shear tests. The adhesive is an elastic–plastic

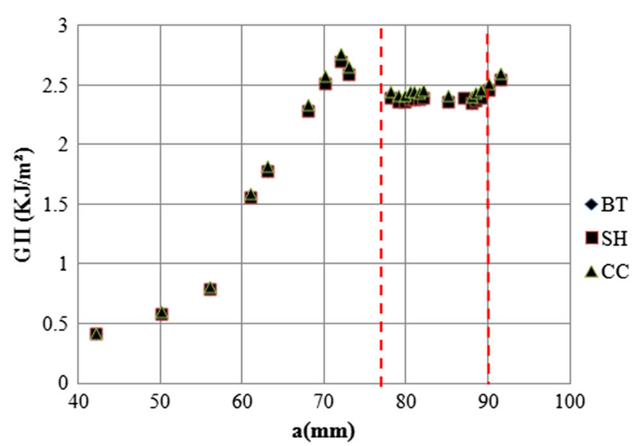

Fig. 8 Energy release rate G_{II} based on the crack propagation

Table 6 Evaluation of critical strain energy release rate (G_{IIC}) for pure mode II

	BT	SH	CC
G_{IIc} (kJ/m^2)	2.39	2.39	2.45
Std (kJ/m^2)	0.095	0.095	0.096

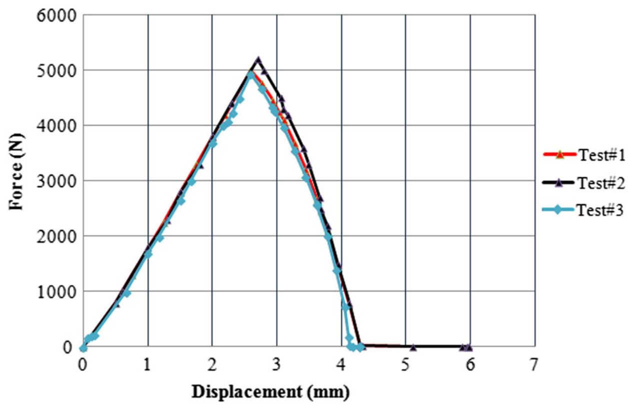

Fig. 9 Force–displacement curve for single lap joints

isotropic material. The steel E24 adherents were modeled using a linear elastic isotropic material model. To simulate cracking behavior in the various experiments, a cohesive zone model was adopted with a bilinear law of traction–separation available in the Abaqus calculation code. The adherents and the adhesive layer were modeled by 2-D plan stress (quadratic elements CPE4) with four nodes. The cohesive elements were modeled by cohesive elements COH2D4 with four nodes, compatible with the elements of CPE4 [23].

3.1.1 Modeling of bonded DCB and ENF tests

A two-dimensional FE model was developed to validate the experimental results of the DCB and ENF tests. The cohesive zone is represented at the substrate–adhesive interface by cohesive elements, or two rows of cohesive elements have been used in the models (DCB and ENF), each row on an interface, Fig. 11.

3.1.2 Modeling of the SLJ shear test

The modeling of the single lap joint is shown in Fig. 12. The substrates are bonded with an adhesive "Adékit A140" of thickness 0.2 mm. The model is embedded at one end, and a displacement was applied on the other side along the direction 1, The mesh size of the cohesive element is 0.02×0.02 mm^2, where the number of cohesive elements is 2500. The number of elements in the model is 19,150. To validate the numerical model, the shear tests were modeled by two models of cohesive zones. In the first model (CZM_i;

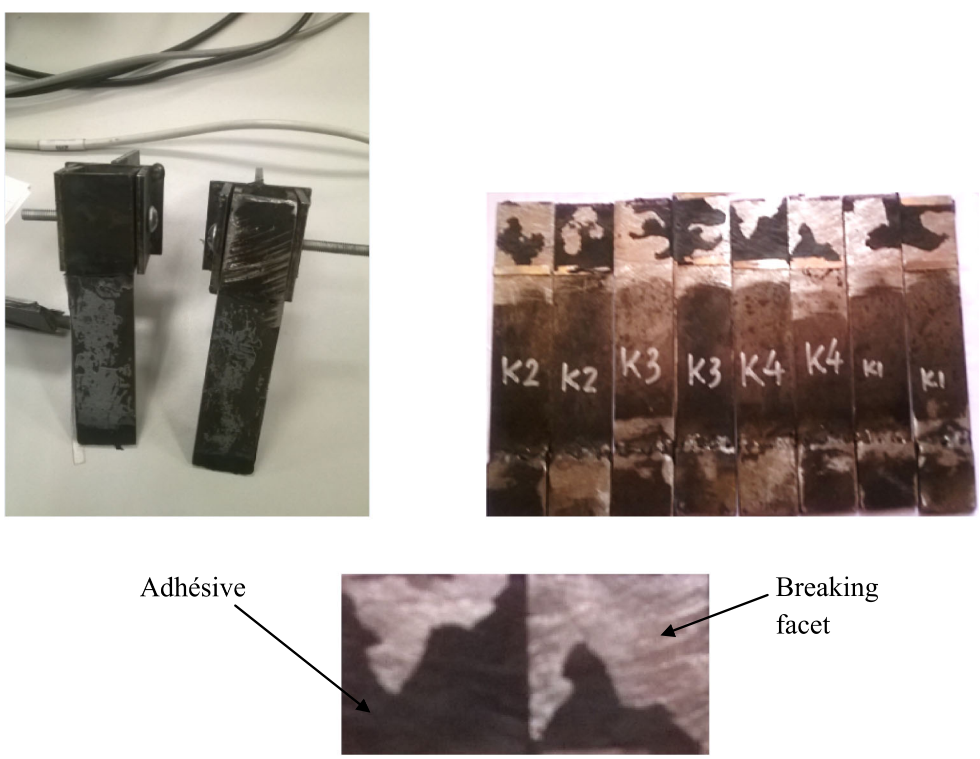

Fig. 10 DCB and SLJ specimens after rupture. **a** DCB specimen after rupture, **b** SLJ specimen after rupture and **c** breaking facet after test

subscript: i = interface), the cohesive elements are arranged on a single interface. On the other hand, the second model (CZM_{ii}) uses two rows of cohesive elements, each arranged on an interface, Fig. 12.

3.2 Description of the CZM model

3.2.1 Cohesive zone model

A cohesive zone model is used to analyze the propagation of cracks. The cohesive zone is defined by cohesive elements where the crack growth will occur. The cohesive law chosen to model the behavior of the adhesive interfaces/substrate is a bilinear traction–separation law proposed by Camanho [24]. The tensile or shear stress (T_i, $i = n$; t) at the interface increases linearly with the opening δ_i, at a slope described by the parameter K representing the initial stiffness of the cohesive zone. When the critical stress $T_{i,\,\max}$ is reached, the interface begins to damage. Finally, the opening between the two lips of the interface reaches a critical value $\delta_{i,m}$ corresponding to the rupture of the interface, Fig. 13. The relationship traction–separation can be expressed as:

$$T_i = (1 - D)K\delta_i, \tag{11}$$

where

$$D = \frac{\delta_{i,m}}{\delta_{i,m} - \delta_{i,0}}\left(1 - \frac{\delta_{i,0}}{\delta_i}\right) \quad \text{if } \delta_i > \delta_{i,0} \quad \text{if not } D = 0$$

D is a damage variable ($0 \leq D \leq 1$). The critical stress $T_{i,\,\max}$, critical opening $\delta_{i,m}$ and energy release rate G_{ic} are linked by the following formula:

$$\mathrm{G}_{\mathrm{ic}} = \frac{T_{i,\max} \times \delta_{i,m}}{2} \tag{12}$$

Under each of the failure modes (pure mode I or pure mode II), the law for describing the behavior of the interface thanks to physical parameters $T_{n,\max}$, G_{Ic} and $\delta_{n,m}$ mode I, and $T_{t,\max}$, $G_{\mathrm{II,c}}$ et $\delta_{t,m}$ mode II is provided (Fig. 12). To model the behavior of an interface in a mixed load, it is necessary to define priming criteria of damage and failure.

3.2.2 Criterion for initiation of damage

A quadratic constraint criterion (QUADS DAMAGE) has been adapted to characterize the initiation of the damage. It involves both the critical tensile stress $T_{n,\max}$ and the critical shear stress $T_{s,\max}$, [25]:

$$\left\{\frac{t_n}{T_{n,\max}}\right\}^2 + \left\{\frac{t_s}{T_{s,\max}}\right\}^2 = 1 \tag{13}$$

The hooks of Macaulay (< >) indicate that only normal traction can initiate damage.

3.2.3 Criterion of damage propagation

A criterion of propagation of damage (Power Law) has been used. It allows us to define the propagation of crack in mode I, mode II and mixed mode I/II. It will be established

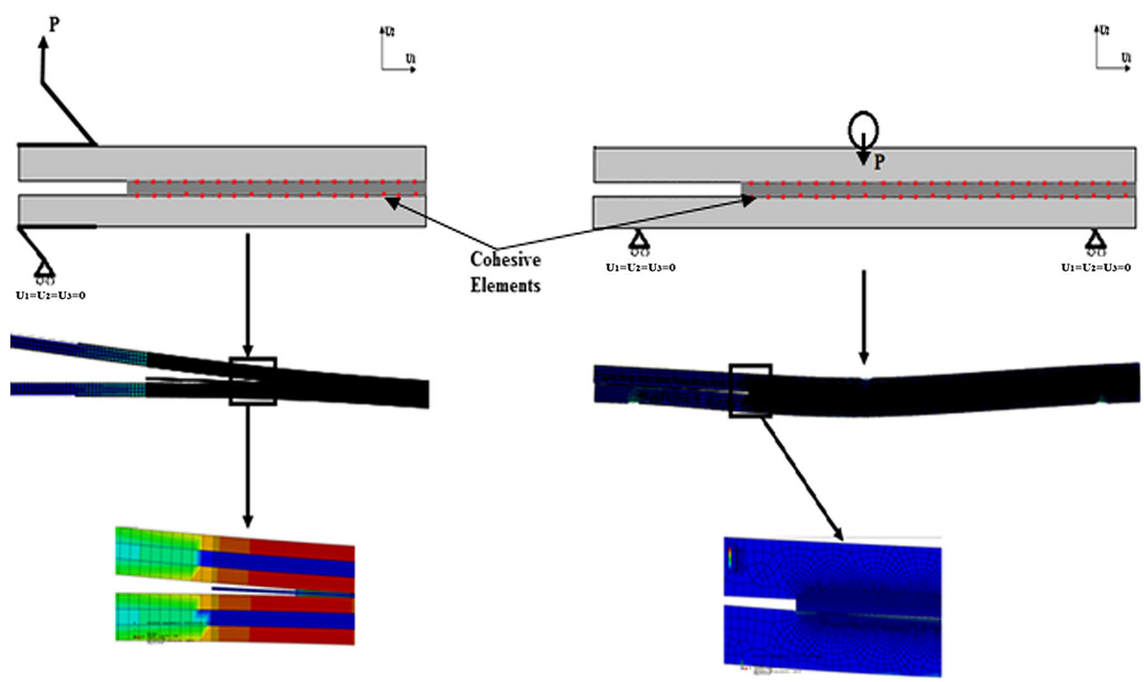

Fig. 11 Damage of joints. **a** DCB model and **b** ENF model

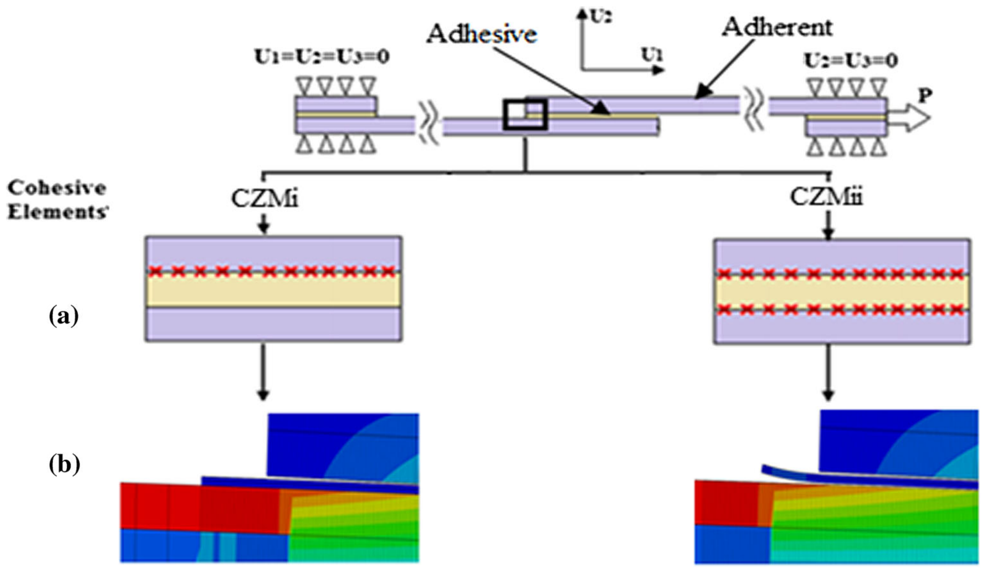

Fig. 12 Modeling of SLJ. **a** Location of rows of cohesive elements in the adhesive joint and **b** cracking failure in joints

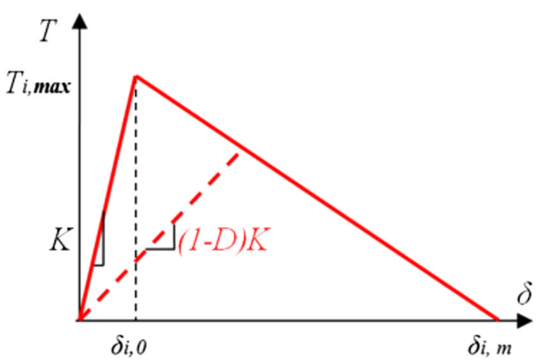

Fig. 13 Bilinear traction–separation law

as a function of the energy release rate G. This law is most widely used in the literature. It involves a parameter α, fixed at 1 for our study:

$$\left[\frac{G_{\mathrm{I}}}{G_{\mathrm{IC}}}\right]^{\alpha}+\left[\frac{G_{\mathrm{II}}}{G_{\mathrm{IIC}}}\right]^{\alpha}=1 \tag{14}$$

3.2.4 Mixed loading

Under a mixed load between the normal and tangential directions, define an equivalent effective displacement and a corresponding effective stress dependent normal value and tangential as follows:

$$\begin{aligned} T_{\mathrm{eq}} &= \sqrt{T_n^2+T_t^2} \\ \delta_{\mathrm{eq}} &= \sqrt{\delta_n^2+\delta_t^2} \end{aligned} \tag{15}$$

The mechanical properties of the adhesive “ADEKIT A140” and cohesive model are summarized in Table 7.

4 Results and discussion

4.1 Fracture modes: DCB and ENF tests

Figure 14 shows the experimental tests and the modeling of the DCB and ENF joints where a cohesive zone model was used with two rows of cohesive elements.

It can be seen in Fig. 13a that the force increases in a linear manner as a function of the imposed displacement without the crack propagating. At the top of the curve, the effort reaches its critical value which then initiates the propagation of the crack. As a result, the stiffness of the specimen decreases, which explains the gradual decrease of effort.

Of the ENF joints tested, four are shown in Fig. 13b. The curves show almost the same behavior and a peak load of 3800 N, followed by a discharge indicating the initiation of the crack which propagates to the total rupture of the joint.

Figure 14 shows a good agreement between experimental and numerical DCB and ENF tests with two rows of cohesive elements.

Table 7 Property of the adhesive “ADEKIT A140” and cohesive model

Material	Properties
Adekit A140	E = 2660Mpa: v = 0.35
Cohesive models	Kn = Ks = 10^7 N/mm^3
	T_n = 35.9 N/mm^2; T_s = 30.9 N/mm^2
	G_{Ic} = 0.5 kJ/m^2; G_{IIc} = 2.41 kJ/m^2

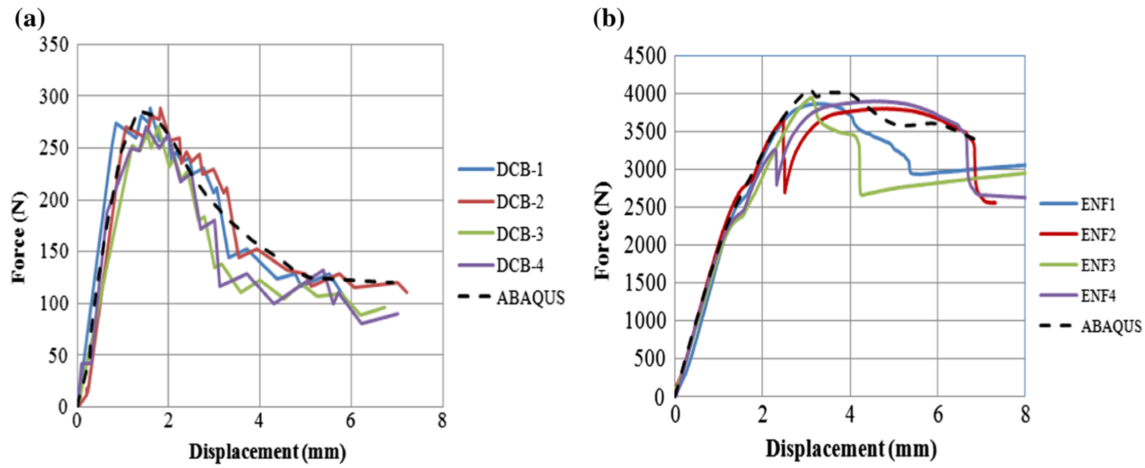

Fig. 14 Comparison of numerical and experimental curves force–displacement tests. **a** DCB and **b** ENF

4.2 Shear test

In order to find the best way to correctly simulate the behavior of a shear test of a bonded joint with an adhesive "Adékit A140" and a bilinear law (TSL), two cohesive zone models were used. The cohesive models are distinguished by the number of rows of cohesive elements used and their geometrical position in the bonded joint, Fig. 12. The properties required for the application of the CZM are identical and are presented in Table 7. Figure 15 represents the numerical results obtained, respectively, by the single-row models (CZM_i) and two rows (CZM_{ii}) of cohesive elements at the interfaces in comparison with the experimental curves of the shear tests. The numerical results show that the rigidity of the joint is inversely proportional to the number of rows of cohesive elements used. Compared with experimental force–displacement curves, the single-row model of cohesive elements (CZM_i), Fig. 15a, has a higher initial stiffness and a slightly lower adhesive joint breakage load. Figure 15b shows a good agreement between the experimental shear test and the two-row modeling of cohesive elements (CZM_{ii}). The modeling of this test, by means of the cohesive law identified beforehand, makes it possible to restore the loading curve and the progress of the rupture process.

The cohesive zone models completely restore the rupture scenario. The number of rows of cohesive elements must respect the number of interfaces in the joint.

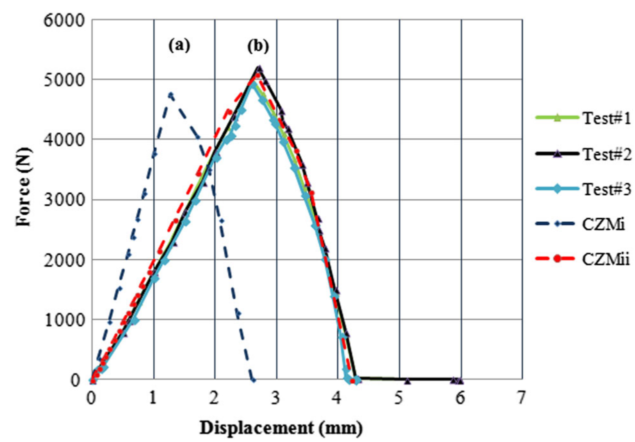

Fig. 15 Experimental and numerical load curves shear tests

5 Conclusion

The aim of this work is to establish a finite element model to simulate cracking failure behavior of a shear test of a bonded joint with an adhesive Adékit A140. The advantage of having a satisfactory finite element model is that it can be used to simulate cases that have not been experimentally tested. A cohesive zone model is used to analyze the propagation of cracks. The cohesive zone is defined by cohesive elements where the progression of the crack will take place. Cohesive zone models using a bilinear traction–separation law have been used because they are best suited to describe crack initiation and propagation in a complex structure, even in the presence of geometric nonlinear behaviors. The comparison of the experimental and numerical results of the mode I test, namely the DCB test, made it possible to identify the two parameters of the cohesive law in mode I that are $T_{n,\max}$ and G_{IC}. In the same way, the modeling of the test in mode II, namely the ENF test, allowed the identification of the parameters of the cohesive law in mode II: $T_{t,\max}$ et G_{IIC}. To model the behavior of an interface under a mixed solicitation mode, all the parameters of the cohesive law were identified and criteria for initiating the damage and rupture were defined. To validate a numerical model allowing to correctly simulate the rupture of the joint, shear tests were modeled by cohesive zone models with one or two rows of cohesive elements. The numerical results compared to the experimental force–displacement curves showed that:

- A model using a row of cohesive elements arranged at the interface (CZM_i) has a higher initial stiffness and a slightly lower adhesive joint breakage load.
- A model using two rows of cohesive elements arranged on the two interfaces (CZM_{ii}) shows good initial stiffness and good resistance to the propagation of the crack in the joints. The "force–displacement" numerical loading curve and the breaking force are in good agreement with experimental loading curves. This model of cohesive zones correctly simulates the experimental force–displacement curve and the course of the rupture process. The number of rows of cohesive elements must respect the number of interfaces in the joint. The force–displacement curves and the numerical fracture scenarios obtained by the cohesive zone models using two rows of cohesive elements are in accordance with the experimental results and allow us to ensure the validity of the cohesive law applied for shear tests of a bonded joint.

References

1. Adams RD, Peppiatt NA (1974) Stress analysis of adhesive-bonded lap joint. J Strain Anal 9:185–196
2. Karachalios EF, Adams RD, daSilva LFM (2013) Single lap joints loaded in tension with high strength steel adherends. Int J Adhes Adhes 43:81–95
3. Essersi O, Tarfaoui M, Boyd S, Shenoi RA, Meraghni F (2011) Experimental study of dynamic behaviour of aluminum/aluminum and composite/composite double lap joints. Appl Mech Mater 62:155–163
4. Tarfaoui M (2011) Prediction of the strength of the adhesively bonded joints by the finite elements method. Appl Mech Mater 62:125–134
5. Adams R, Atkins R, Harris J, Kinloch A (1986) Stress analysis and failure properties of carbon-fibre reinforced plastic/steel double lap-joint. J Adhes 20:29–30
6. Seong MS, Kim TH, Nguyen KH, Kweon JH, Choi JH (2008) A parametric study on the failure of bonded single-lap joints of carbon composite and aluminum. Compos Struct 86:135–145
7. Tsai M, Morton J, Matthhews FL (1995) Experimental and numerical studies of a laminated composite single-lap adhesive joint. J Compos Mater 29(9):1254–1275
8. Tsai M (1995) The effect of a spew fillet on adhesive stress distributions in laminated composite single-lap joints. Compos Struct 32:123–131
9. Apalak Z, Apalak M, Genc M (2006) Progressive damage modeling of an adhesively bonded unidirectional composite single-lap joint in tension at the mesoscale level. J Thermoplast Compos Mater 19:671–702
10. Da Silva LFM, Campilho RDSG (2011) Advances in numerical modelling of adhesive joints. Springer, Heidelberg
11. Feraren P, Jensen HM (2004) Cohesive zone modelling of interface fracture near flaws in adhesive joints. Eng Fract Mech 71:2125–2142
12. Hamitouche L, Tarfaoui M, Vautrin A (2008) An interface debonding law subject to viscous regularization for avoiding instability: application to the delamination problems. Eng Fract Mech 75(10):3084–3100
13. Crocombe A, Hua Y, Loh W, Wahab M, Ashcroft I (2006) Predicting the residual strength for environmentally degraded adhesive lap joints. Int J Adhes Adhes 26:325–336
14. Borg RL, Simonsson K (2004) Simulating DCB, ENF and MMB experiments using shell elements and a cohesive zone model. Compos Sci Technol 64(2):269–278
15. Valoroso N, Sessa S, Lepore M, Cricrì G (2013) Identification of mode-I cohesive parameters for bonded interfaces based on DCB test. Eng Fract Mech 104:56–79
16. Alfredsson KS (2004) On the instantaneous energy release rate of the end-notch flexure adhesive joint specimen. Int J Solids Struct 41:4787–4807
17. Leffler K, Alfredsson KS, Stigh U (2007) Shear behaviour of adhesive layers. Int J Solids Struct 44:520–545
18. Hashemi S, Kinloch AJ, Williams JG (1990) The analysis of interlaminar fracture in uniaxial fibre–polymer composites. Proc R Soc Lond A Math Phys Sci 427(1872):173–199
19. Blackman B, Dear JP, Kinloch AJ, Osiyemi S (1991) The calculation of adhesive fracture energies from double-cantilever beam test specimens. J Mater Sci Lett 10:253–256. https://doi.org/10.1007/BF00735649
20. deMoura MFSF, Gonc-alves JPM, Magalhaes AG (2012) A straightforward method to obtain the cohesive laws of bonded joints under mode I loading. Int J Adhes Adhes 39:54–59
21. Berry JP (1960) Some kinetic considerations of the Griffith criterion for fracture II: equations of motion at constant deformation. J Mech Phys Solids 8(3):207–216
22. Berry JP (1963) Determination of fracture surface energies by the cleavage technique. J Appl Phys 34:62–68
23. ABAQUS/Standard (2014) User's manual, version 6.14.1. HKS Inc., Dallas
24. Camanho PP, Davila CG (2002) Mixed-mode decohesion finite elements for the simulation of delamination in composite materials. National Aeronautics and Space Administration, NASA/TM-2002-211737
25. Campilho RDSG, de Moura MFSF, Ramantani DA, Morais JJL, Domingues JJMS (2009) Buckling behaviour of carbon–epoxy adhesively-bonded scarf repairs. J Adhes Sci Technol 23:1493–1513